Steady-state shear flows via nonequilibrium molecular dynamics and smooth-particle applied mechanics

Harald A. Posch

Institute for Experimental Physics, University of Vienna, Boltzmanngasse 5, Wien A-1090, Austria

William G. Hoover and Oyeon Kum

*Department of Applied Science, University of California at Davis/Livermore and Lawrence Livermore National Laboratory,
Livermore, California 94551-7808*

We simulate both microscopic and macroscopic shear flows in two space dimensions using nonequilibrium molecular dynamics and smooth-particle applied mechanics. The time-reversible *microscopic* equations of motion are isomorphic to the smooth-particle description of inviscid *macroscopic* continuum mechanics. The corresponding microscopic particle interactions are relatively weak and long ranged. Though conventional Green-Kubo theory suggests instability or divergence in two-dimensional flows, we successfully define and measure a finite shear viscosity coefficient by simulating stationary plane Couette flow. The special nature of the weak long-ranged smooth-particle functions corresponds to an unusual kind of microscopic transport. This microscopic analog is mainly kinetic, even at high density. For the soft Lucy potential which we use in the present work, nearly all the system energy is potential, but the resulting shear viscosity is nearly all kinetic. We show that the measured shear viscosities can be understood, in terms of a simple weak-scattering model, and that this understanding is useful in assessing the usefulness of continuum simulations using the smooth-particle method. We apply that method to the Rayleigh-Bénard problem of thermally driven convection in a gravitational field.

I. INTRODUCTION

Boltzmann popularized the quest for an understanding of the emergence of irreversibility from time-reversible equations of motion. His explanation made it plain that irreversible behavior can be seen in isolated systems only if fluctuations are ignored—that is, ensemble averages can approach equilibrium even while individual histories continue to cover all available states. Generalizing classical mechanics, admitting interactions with the surrounding world, to include sources and sinks of work and heat, has two advantages: (i) stationary nonequilibrium states can then be generated, and (ii) the analysis of irreversibility becomes less difficult. Several methods for treating time-reversible heat reservoirs have established that the irreversibility associated with the conversion of work to heat is rooted in the chaotic instability of the underlying motion equations [1,2]. The Green-Kubo theory [3], which predicts irreversible behavior in terms of the ensemble average of equilibrium correlation functions, is a general demonstration of the possibility of obtaining irreversible behavior from reversible motion equations.

It has been widely accepted that the Green-Kubo theory predicts some kind of divergence for two-dimensional transport coefficients [4]. The diffusion coefficient, viscosities, and heat conductivity were all expected to diverge because the corresponding correlation integrals decay slowly in two dimensions, inversely as the time. On the other hand, recent high-precision simulations [5] of shear flow, for a short-ranged steep repulsive potential produced a size-independent, though rate-

dependent, shear viscosity fairly close to the predictions of Gass' two-dimensional Enskog theory [6]. The reproducible finite nature of these viscosities could be made understandable if the coefficients only diverge in some unobtainable zero-rate large-system limit. Evidently, the simple Green-Kubo derivation of divergence fails to hold for finite systems with finite steady nonequilibrium fluxes. The simulations we report here, for a very different potential, show no problems in defining and using viscosity in two dimensions and cast doubt on the generality of the divergence argument.

An interesting additional puzzle emerged when we began to use *smoothed-particle methods* to solve analogous flow problems in continuum mechanics. In this approach [7] the equations of continuum mechanics are smoothly interpolated in space, using summed contributions from a set of moving material points. The continuum field variables—stress, energy, strain rate, and heat flux—anywhere in space are calculated by superposing the contributions from all those moving points, which lie within the range of a *weight function* which describes the "smoothing." At a given space point the superposed averages usually involve contributions from a few dozen of the moving points.

If the continuum material we choose to model happens to be a two-dimensional ideal gas, then the corresponding inviscid Euler equations have as their smooth-particle representation the motion of particles obeying the usual equations of molecular dynamics, with the weight function playing the role of an interatomic potential [8]. Thus, the smooth-particle approach to continuum

mechanics produces another version of the paradox Boltzmann studied: linking reversible particle motion equations to irreversible macroscopic behavior [9].

Though the irreversibility problem is an old one, the capacity and speed of present day computers makes this a good time to investigate all these questions anew, beginning with both equilibrium Green-Kubo and nonequilibrium steady-state Couette flow simulations of two-dimensional viscosities, and then applying the results to the simulation of a two-dimensional unstable flow, the Rayleigh-Bénard problem. In Sec. II, we introduce the smooth-particle approach to continuum simulations, stressing the parallels linking this continuum approach to molecular dynamics in the case that the macroscopic weight function is proportional to the microscopic potential function. Because the atomistic view is unique, and underlies the continuum one, we next consider atomistic particles, describing in Sec. III how the continuum constitutive relation linking stress and strain rate can be obtained from atomistic simulations of plane Couette flow. In Sec. IV, we exploit the close relationship linking smooth-particle applied mechanics and molecular dynamics to compute the viscous shear response of a particular ideal fluid, which can be pictured in either an atomistic or a continuum point of view. Section V contains a comparison of the nonequilibrium viscosities for this case with equilibrium estimates from Green-Kubo theory. In Sec. VI, we explore a nonlinear problem, heat-induced convection in a gravitational field (the Rayleigh-Bénard problem). Section VII records our conclusions.

II. SIMULATION OF FLOWS USING SMOOTH-PARTICLE APPLIED MECHANICS

Smoothed-particle applied mechanics (SPAM) provides an *ordinary*-differential-equation *particle* method [7–11] for solving the partial differential conservation equations of *continuum* mechanics:

$$d\rho/dt = -\rho\nabla\cdot\mathbf{v} \ ;$$
$$\rho d\mathbf{v}/dt = \nabla\cdot\sigma \ ; \tag{2.1}$$
$$\rho de/dt = \sigma:\nabla\mathbf{v} - \nabla\cdot\mathbf{Q} \ .$$

The method, often called smooth-particle "hydrodynamics," can be applied to solids as well as to fluids. It treats the motion of N "smoothed," or "smeared-out," particles, distributed in space. All the field variables in the continuum conservation equations, including the mass density ρ, the velocity $\mathbf{v}$, the energy per unit mass e, the stress tensor σ, and the heat flux vector $\mathbf{Q}$, are interpolated among the locations of the moving particles. In the simplest form of the theory, the density at any point in space, $\rho(\mathbf{r})$, is given by the summed contribution of all particles within range of that point:

$$\rho(\mathbf{r}) = m \sum_j w(\mathbf{r} - \mathbf{r}_j) \ . \tag{2.2}$$

The density at the position of any particle includes the self-term $w(0)$, from the term $i = j$ in the sum over j:

$$\rho_i = \rho(\mathbf{r}_i) = m \sum_j w(\mathbf{r}_i - \mathbf{r}_j) = m \sum_j w(\mathbf{r}_{ij}) \ ; \quad \mathbf{r}_{ij} = \mathbf{r}_i - \mathbf{r}_j \ . \tag{2.3}$$

The motion of particle i is governed by the stress tensor and the "weighting," or "smearing," or "smoothing" function $w(r)$, in a sum over all nearby particles j:

$$d^2\mathbf{r}_i/dt^2 = d\mathbf{v}_i/dt$$
$$= \sum_j [(m\sigma/\rho^2)_i + (m\sigma/\rho^2)_j]\cdot\nabla_i w(\mathbf{r}_{ij}) \ , \tag{2.4}$$

where the stress σ_i at each particle is calculated from its internal energy per unit mass, e_i (which obeys a similar equation) and its mass density ρ_i.

We use a special weighting function, $w(\mathbf{r}) = w_{\text{Lucy}}(\mathbf{r})$, in this work. It is typical of such functions, being smooth, monotone decreasing with increasing r, and designed to include interactions between each particle and a few tens of nearby neighbors. It was used by Lucy [11], who, with Monaghan [7], invented the smoothed-particle method in 1977. This Lucy weight function has circular symmetry, and exactly the same analytic form, apart from the units, as does the Lucy potential function which we use in Sec. IV:

$$w_{\text{Lucy}}(r < h = 3\sigma) = (5/h^2\pi)[1 + (3r/h)][1 - (r/h)]^3 \ . \tag{2.5}$$

We arbitrarily choose the cutoff, or range, of this function to be $h = 3\sigma$. The multiplicative constant $(5/\pi h^2) = (5/9\pi\sigma^2)$ is then fixed by the two-dimensional normalization of w: $\int 2\pi r w \, dr = 1$.

Note that a scalar equation of state, for a two-dimensional ideal gas,

$$-\sigma_{xx} = -\sigma_{yy} = P = \rho e = P_o(\rho/\rho_o)^2/2 \ , \tag{2.6}$$

(where $P_o = \varepsilon/\sigma^2$ and $\rho_o = m/\sigma^2$ are constants) provides equations of motion *isomorphic* to the motion equations of monatomic molecular dynamics [7],

$$\{m\ddot{\mathbf{r}}_i = m\dot{\mathbf{v}}_i = -\nabla_i\Phi\} \ , \quad \Phi = \sum\phi(\mathbf{r}_{ij}) \ , \tag{2.7}$$

where $\phi(r)$ is the pair potential. These equations constitute an autonomous set, with a solution independent of the energy equation. [The energy equation (2.1), with $\mathbf{Q}$ set equal to 0, is, however, fully consistent with the dynamics generated by (2.7).] Thus, the smooth particles, whose motion is governed by the ideal gas pressure tensor, through the weighting function $w(\mathbf{r})$, trace out the same trajectories as would atomistic particles governed, through the corresponding potential function $\phi(r)$, by the equations of molecular dynamics. For definiteness, we continue with our special, though typical, choice of the potential corresponding to our smoothed-particle weighting function, using again the functional form introduced by Lucy: $\phi_{\text{Lucy}}(\mathbf{r}) = (\varepsilon\sigma^2)w_{\text{Lucy}}(\mathbf{r})$. Potential functions de-

rived from weighting functions, such as this, differ, in shape, range, and units, from conventional pair potentials $\phi(r)$. Because the smoothed-particle function has no strongly repulsive core and is also relatively long ranged, each smoothed particle simultaneously interacts, weakly, with dozens of others. The statistical mechanics and hydrodynamics of corresponding long-ranged molecular systems, with pair potentials resembling Lucy's weighting function, have not yet been systematically explored.

Energy is reckoned a little differently in the microscopic and macroscopic dynamics. In the smooth-particle density and energy sums, the self-contribution of each particle, proportional to $w(0)$, *is* included. In the molecular dynamics simulations of Sec. IV, the corresponding contributions to the energy,

$$\{\phi_{\text{Lucy}}(\mathbf{r}_{ii}=0)=(\varepsilon\sigma^2)w_{\text{Lucy}}(0)$$

$$=(5\varepsilon\sigma^2/\pi h^2)=0.1768\,388\varepsilon\} , \quad (2.8)$$

are not included. This difference does not affect the isomorphism of the two kinds of particle trajectories, since $w'(0)$ and $\phi'_{\text{Lucy}}(0)$ both vanish.

In this paper, we apply molecular dynamics, equivalent to ideal-gas smoothed-particle applied mechanics, to the analysis of simple two-dimensional flows. We consider first plane Couette flow and then convective Rayleigh-Bénard flow, in which convection rolls, driven by heating in a gravitational field, compete with conduction, as a mechanism for heat transfer. The lack of viscosity for the continuum ideal-gas version of this model suggests that the corresponding flows describe the large-Reynolds-number limit of turbulence analyses [12–14]. It is paradoxical that there is an intrinsic atomistic viscosity present in the implementation of this continuum model, which prevents that model's Reynolds number from diverging.

Movies of smoothed-particle flows reveal high-frequency velocity fluctuations, which are ordinarily absent in continuum mechanics. Because the particles can be large, the smooth-particle simulation method has a substantial scale advantage over molecular dynamics.

III. SIMULATION OF STEADY TWO-DIMENSIONAL PLANE COUETTE FLOW

Homogeneous periodic shear has been studied for more than 20 years [2,5,15]. In such a flow, an N-particle system is driven by the motion of neighboring periodic image systems, as shown in Fig. 1. From the macroscopic standpoint, and confirmed by the microscopic equations of motion, the sheared system would steadily gain energy, and heat up, due to this periodic boundary driving. To avoid this heating, and to obtain a nonequilibrium steady state, it is usual to add time-reversible Gauss [16] or Nosé-Hoover [17,18] "friction coefficients" ζ to the equations of motion. The resulting reversible friction constrains or controls either the temperature or the internal (excluding the macroscopic flow kinetic energy) energy.

For two-dimensional particles of mass m, and with a macroscopic strain rate $\dot{\varepsilon}=du_x/dy$, the Gaussian *isoenergetic* form of these equations that we use here is the set
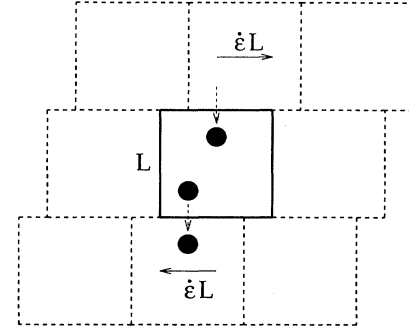

FIG. 1. Two-dimensional $L\times L$ plane Couette shear flow driven by the relative motion of periodic images (shown dashed). This periodic driving, "Lees-Edwards boundary conditions," is augmented by a global ergostat in order to generate a nonequilibrium steady state.

$$\{\dot{x}=\dot{\varepsilon}y+(p_x/m) \ ; \quad \dot{y}=(p_y/m) \ ; $$

$$\dot{p}_x=F_x-\dot{\varepsilon}p_y-\zeta p_x \ ; \quad \dot{p}_y=F_y-\zeta p_y\} , \quad (3.1)$$

with

$$\zeta=-\dot{\varepsilon}P_{xy}V/2K \ ; \quad K=(1/2m)\sum p^2 . \quad (3.2)$$

P_{xy} is the xy component of the pressure tensor and K is the kinetic energy, measured in terms of particle velocities relative to the mean flow. The isokinetic version of these equations has been called the "Sllod" algorithm because of its close relationship to the Dolls Tensor algorithm [19]. The friction coefficient ζ extracts heat from the system at exactly the rate that the periodic shearing boundaries do thermodynamic work on the system,

$$\dot{W}=\dot{\varepsilon}P_{xy}V . \quad (3.3)$$

In our numerical simulations we derive the interparticle forces in the motion equations $\{(F_x,F_y)=-\nabla\Phi\}$ from the specially chosen short-ranged Lucy pair potential shown in Fig. 2:
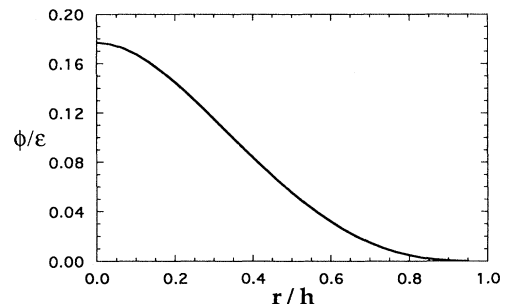

FIG. 2. Lucy potential function, ϕ_{Lucy}, proportional to the weighting function which we use in our smooth-particle applied mechanics simulations here. The integral of the weighting function is normalized to unity. The force from the Lucy potential vanishes quadratically at the cutoff. In our two-dimensional simulations, each fluid particle interacts with approximately 30 others.

$$\phi_{\text{Lucy}}(\mathbf{r}) = (5\varepsilon\sigma^2/h^2\pi)[1+(3r/h)]$$

$$\times[1-(r/h)]^3 \quad \text{for } r < h = 3\sigma \ . \qquad (3.4)$$

The reason for this particular choice, which contains the energy scale ε, the length scale σ, and the cutoff range h, is described more fully in Sec. IV. As usual, the total potential energy Φ is a sum of pair contributions $\{\phi_{ij}\}$, one for each pair of particles closer than the cutoff distance. Throughout this work, we arbitrarily choose the range of the potential, h, equal to 3σ and the volume per particle equal to σ^2, giving the relations $h = 3\sigma = 3(V/N)^{1/2}$. Here N is the number of particles in the simulation and V is the volume. As before [5], we use the linked-list method in combination with Lees-Edwards boundary conditions for the intergration of the equations of motion.

IV. SHEAR VISCOSITIES FOR LUCY'S FORM OF $\phi(\mathbf{r})$ AND $w(\mathbf{r})$

It is convenient to solve the set of $4N$ motion equations for $\{\dot{x}, \dot{y}, \dot{p}_x, \dot{p}_y\}$ using the classic fourth-order Runge-Kutta method. We have previously simulated the viscous properties for a short-ranged steeply repulsive force using this method [5]. Here, the quadratic nature of our force cutoff implies discontinuities in the forces, proportional to dt^2, leading to local single-step trajectory errors of order dt^4. These exceed the Runge-Kutta integration error, which is of order $dt^5/5!$. With a time step of $0.005(m\sigma^2/\varepsilon)^{1/2}$, the single-step energy is still conserved to about 12 digit accuracy. This small energy error can be eliminated by rescaling the momenta after each Runge-Kutta integration step.

All of our simulations have been carried out at unit reduced density, $N\sigma^2 = V$. This choice gives 24 interacting neighbors for each particle when the particles are arranged in a regular square lattice and 36 interacting neighbors when the particles are arranged in a regular triangular lattice. We use two different energies, $N\varepsilon/2$ and $N\varepsilon$. It turns out that in the first lower-energy case, the energy is mainly potential, with $kT \approx 0.07\varepsilon$, less than half the potential height, $(\varepsilon\sigma^2)w(0) = \phi(0) = 5\varepsilon/(9\pi)$. The higher-energy case, with $E = \Sigma m[e + (v^2/2)] = N\varepsilon$, corresponds to a thermal energy $kT \approx 0.54\varepsilon$, three times the maximum value of the potential.

Typical instantaneous *configurations* of 1024 smoothed particles are shown in Fig. 3 for the two choices of the total energy, $N\varepsilon/2$ (left) and $N\varepsilon$ (right), at the moderately high strain rate, $\dot{\varepsilon} = (\varepsilon/m\sigma^2)^{1/2}$. Although they appear to be very similar, a striking difference can best be displayed by using an analysis of these structures, suggested to us by Davé. If the local dyadic sum at $\mathbf{r}$,

$$S_{\text{Davé}}^{xx}(\mathbf{r}) = \sum \Delta y_i \Delta y_i w(\mathbf{r}_i - \mathbf{r}) \ ;$$

$$S_{\text{Davé}}^{yy}(\mathbf{r}) = \sum \Delta x_i \Delta x_i w(\mathbf{r}_i - \mathbf{r}) \ ;$$

$$S_{\text{Davé}}^{xy}(\mathbf{r}) = S_{\text{Davé}}^{yx}(\mathbf{r}) = -\sum \Delta x_i \Delta y_i w(\mathbf{r}_i - \mathbf{r}) \ ;$$

$$\Delta \mathbf{r}_i = \mathbf{r}_i - \mathbf{r} \ ;$$
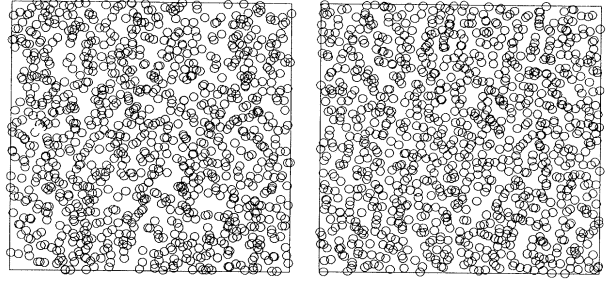
resembling a moment-of-inertia tensor, is diagonalized,

FIG. 3. Typical configuration of 1024 Lucy particles undergoing shear, at unit reduced strain rate, with per-particle internal energies of 0.5ε (left) and 1.0ε (right).

and a path is traced out in the direction of the eigenvector belonging to the minimum eigenvalue, the system is neatly divided into a set of cells, as is shown in Fig. 4.

To draw these pictures, N points on a regular grid covering the simulation box were chosen as starting points for paths of 200 iterations and a step size of 0.1σ per iteration. The sign of the eigenvector at the initial points was chosen randomly. At any point farther along the path it was chosen such that the scalar product of the eigenvectors for successive steps be positive. The last 150 iterations were used in constructing Fig. 4. Motion along the paths can be viewed as a constant-speed "flow" with characteristic strain-rate-dependent mean-squared displacements, $\langle (\Delta x)^2 \rangle$ and $\langle (\Delta y)^2 \rangle$. The x and y directions are, respectively, parallel and perpendicular to the flow. This idea is used in Fig. 5 for the same two examples. Each curve is an average over at least 150 instantaneous configurations (taken at intervals of 200 Runge-Kutta time steps). The limiting slopes of these curves correspond to strain-rate-dependent "diffusion coefficients," but with units of σ, because the "time" along the path is measured in σ units. At unit reduced strain rate, we find $\{D^x, D^y\}$ is $\{1.05, 3.83\}$ for $E = N\varepsilon/2$ and $\{1.00, 3.21\}$ for $E = N\varepsilon$. As one might expect, the mean-squared displacement in the shear direction is practically energy independent, but varies significantly in the perpendicular direction.

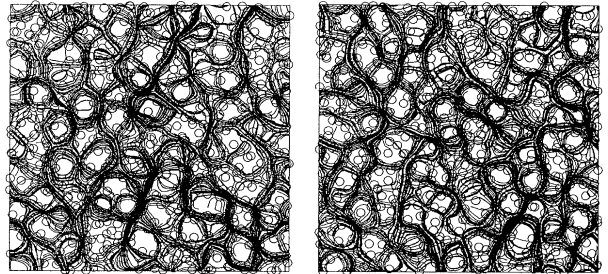The structural anisotropicity introduced by the shear-

FIG. 4. Topological analysis, using Davé's suggestion, of the configurations of 1024 Lucy particles undergoing shear, at unit reduced strain rate, with per-particle internal energies of 0.5ε (left) and 1.0ε (right).
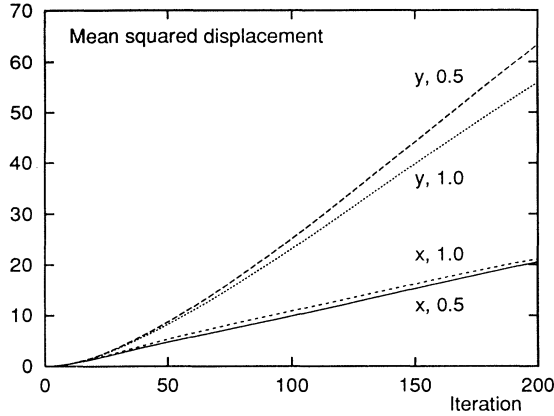
FIG. 5. Mean-squared displacements, divided by σ^2, for the artificial "flow" used to characterize the topology of sheared systems. The shearing motion is parallel to the x axis. Both the direction of the measured displacements (x or y) and the reduced strain rate (0.5 or 1.0) have been used to label the curves. Each "iteration" corresponds to a path increment of 0.1σ, as described in Sec. IV.

ing is very pronounced, though it is hardly discernable in the instantaneous configurations shown in Fig. 3. The anisotropy vanishes in the shear-free case, but the energy dependence persists, as shown in Fig. 6, where we have combined the two directions. We find that the diffusion coefficients are 1.6, for $E=N\varepsilon/2$, and 2.1 for $E=N\varepsilon$. This analysis can be modified by permitting the step size (here 0.1σ) to depend upon the local values of the eigenvalues of matrix (4.1). This approach might be useful for the characterization of totally different systems, such as polymers.

Though we do not show them here, it is important to emphasize that velocities, in smooth-particle applied mechanics, can be interpreted in terms of two different momenta: the individual particle "momenta" $\{\mathbf{p}_i\}$, which represent velocities relative to the mean streaming motion

$$\{\mathbf{p}_i\}=m\{\mathbf{v}_i-(\dot{\varepsilon}y,0)\} , \qquad (4.2)$$

and the averaged momenta $\{\langle\mathbf{p(r)}\rangle=\sigma^2\sum w(\mathbf{r}-\mathbf{r}_j)\mathbf{p}_j\}$, which can be evaluated at any point, and are computed using the weighting function. The averaged momenta $\{\langle\mathbf{p}_r\rangle\}$ can, for instance, be computed on a square grid to facilitate the calculation of (fast) Fourier transforms of the velocity field, and so are a more useful representation of the flow than are the individual particle momenta.

We have carried out a wide range of calculations in order to determine the viscous response of Lucy's fluid as a function of strain rate at two different energies. The resulting pressure tensors and potential energies (omitting the contributions from the self-term at $r=0$) are given in Tables I and II. The rate-dependent shear viscosities, $\{\eta=-P_{xy}/\dot{\varepsilon}\}$ from these data are displayed in Fig. 7. In Fig. 8, we show also the normal stress function, $\langle P_{xx}-P_{yy}\rangle/\dot{\varepsilon}^2$. The data indicate that the Lucy "fluid" exhibits noticeable shear thinning at strain rates in excess
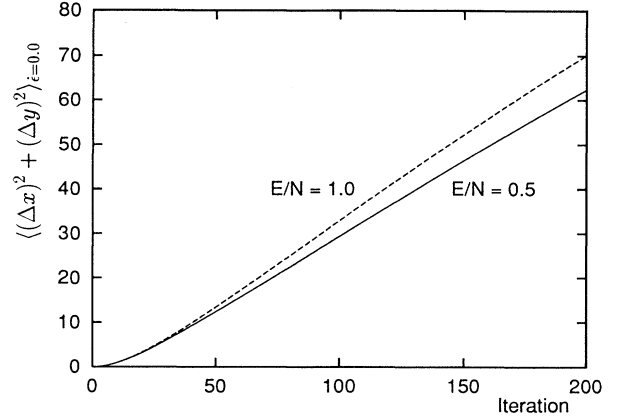

FIG. 6. Combined mean-squared displacements (x plus y), divided by σ^2, as a function of energy for the equilibrium zero-strain-rate case.

of $0.01(\varepsilon/m\sigma^2)^{1/2}$ and that the viscosity is sensitive to temperature, varying roughly as $T^{3/2}$ in the range considered here. An extremely interesting feature of the data at the higher energy, $E=N\varepsilon$, is an instability occurring in the strain-rate range $\dot{\varepsilon}\approx(0.010\pm0.002)(\varepsilon/m\sigma^2)^{1/2}$. Though we have not investigated this instability in exhaustive detail, its symptom is that a single particle fairly rapidly attains most of the system kinetic energy. The instability is presaged by dramatic fluctuations in the shear stress $\langle -\sum p_x p_y/mV\rangle$.

The trajectories traced out by the particles are exactly the same, whether molecular dynamics, or smooth-particle continuum mechanics is used. Likewise, the kinetic part of the shear pressure-tensor component according to molecular dynamics, $(1/mV)\langle\sum p_x p_y\rangle$, corresponds to the negative of a volume-averaged Reynolds stress in the continuum, $\langle -\rho v_x v_y\rangle$, measured in the comoving frame. On the other hand, the potential part
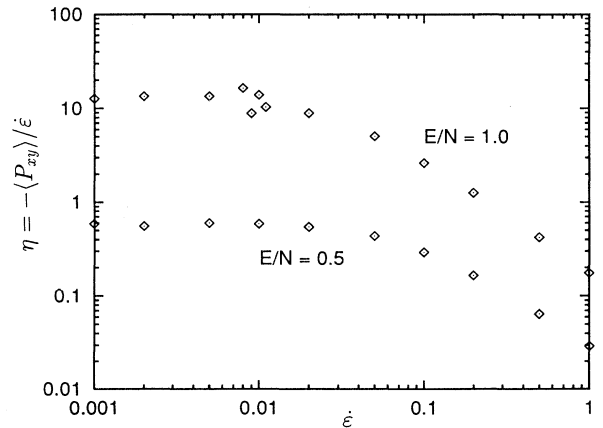

FIG. 7. Dependence of shear viscosity, divided by $(m\varepsilon)^{1/2}/\sigma$, on strain rate for $E=N\varepsilon$ and $E=N\varepsilon/2$. These results are for thermostatted systems of 1024 Lucy particles. Note the instability, discussed in the text, at reduced strain rates near 0.01 in the higher-energy case.

TABLE I. Kinetic and potential parts of the stress tensor for Lucy's potential $\phi(r<h=3\sigma)=(5\varepsilon\sigma^2/\pi h^2)[(1+(3r/h)][1-(r/h)]^3$ using a Gaussian ergostat imposing a fixed total energy $E=\sum\phi(r_{ij})+\sum(p^2/2m)=N\varepsilon/2$. The container is square, with $V=N\sigma^2$. The potential energy is given; the kinetic and potential parts of the pressure tensor are arranged in pairs {kinetic,potential}. The time step in the fourth-order Runge-Kutta simulations was $0.005(m\sigma^2/\varepsilon)^{1/2}$. A simulation of the Green-Kubo viscosity with $N=1024$ and for an elapsed time of 20 000 provided the estimate $\eta=0.548(m\varepsilon)^{1/2}/\sigma$ with a hydrostatic pressure of $0.5562(\varepsilon/\sigma^2)$, of which $0.071(\varepsilon/\sigma^2)$ is the kinetic contribution. In giving these numerical results we have chosen units with $m=1$, $\varepsilon=1$, and $\sigma=1$. The total time of the run is expressed in units of $\tau=1/\dot\varepsilon$.

N	t/τ	$\dot\varepsilon$	$\langle\Phi/N\varepsilon\rangle$	$\langle P_{xy}\rangle$		$\langle P_{xx}\rangle$		$\langle P_{yy}\rangle$	
1024	28	0.001	0.429	−0.0006	+0.0001	+0.0714	+0.4849	+0.0714	+0.4849
1024	27	0.002	0.429	−0.0012	+0.0001	+0.0715	+0.4848	+0.0713	+0.4848
1024	108	0.005	0.429	−0.0032	+0.0003	+0.0715	+0.4848	+0.0712	+0.4849
1024	40	0.010	0.429	−0.0063	+0.0005	+0.0721	+0.4846	+0.0708	+0.4849
1024	80	0.020	0.428	−0.0119	+0.0010	+0.0736	+0.4845	+0.0696	+0.4848
400	90	0.050	0.428	−0.0232	+0.0016	+0.0806	+0.4836	+0.0642	+0.4853
1024	221	0.050	0.428	−0.0233	+0.0016	+0.0808	+0.4837	+0.0639	+0.4853
1024	614	0.100	0.427	−0.0305	+0.0014	+0.0908	+0.4824	+0.0546	+0.4864
1024	304	0.200	0.428	−0.0325	+0.0005	+0.1012	+0.4813	+0.0432	+0.4883
400	575	0.500	0.431	−0.0272	+0.0048	+0.1082	+0.4774	+0.0290	+0.4907
1024	500	0.500	0.431	−0.0274	+0.0048	+0.1081	+0.4773	+0.0291	+0.4908
4096	320	0.500	0.431	−0.0273	+0.0048	+0.1083	+0.4774	+0.0290	+0.4907
400	500	1.000	0.442	−0.0214	+0.0075	+0.0951	+0.4719	+0.0209	+0.4935
1024	760	1.000	0.442	−0.0218	+0.0074	+0.0941	+0.4724	+0.0212	+0.4936
4096	470	1.000	0.442	−0.0218	+0.0074	+0.0945	+0.4723	+0.0210	+0.4936

of the molecular stress has no simple continuum analog. In most of the cases appearing in Tables I and II this contribution to the shear stress is barely significant.

The small-strain-rate viscosities found at the two energies considered can be estimated on the basis of a simple argument. Imagine that the thermal velocity, $(kT/m)^{1/2}$ is gradually degraded by a fluctuating random force F_{random} (which would vary as the mean slope of the Lucy potential function multiplied by the square root of the number of interacting neighbors). Because the direction

of this force is random, the decay time should vary as the square of the ratio $(kT/m)^{1/2}/F_{random}$. The resulting estimate for the kinematic viscosity, $\lambda v/3$, where λ is the mean free path, turns out to vary as $T^{3/2}$. This argument describes the temperature dependence of our viscosities very well and also provides semiquantitative agreement with the numerical values

$$\eta=35(mkT)^{1/2}(kT/\varepsilon\sigma) ,\qquad(4.3)$$

restricted to the case of unit number density, $N\sigma^2=V$.

TABLE II. Kinetic and potential parts of the stress tensor for Lucy's potential $\phi(r<h=3\sigma)=(5\varepsilon\sigma^2/\pi h^2)[(1+(3r/h)][1-(r/h)]^3$ using a Gaussian ergostat imposing a fixed total energy $E=\sum\phi(r_{ij})+\sum(p^2/2m)=N\varepsilon$. The container is square, with $V=N\sigma^2$. The potential energy is given; the kinetic and potential parts of the pressure tensor are arranged in pairs {kinetic,potential}. The time step in the fourth-order Runge-Kutta simulations was $0.005(m\sigma^2/\varepsilon)^{1/2}$. A simulation of the Green-Kubo viscosity with $N=1024$ and for an elapsed time of 40 000 provided the estimate $\eta=14.0(m\varepsilon)^{1/2}/\sigma$ with a hydrostatic pressure of $1.024(\varepsilon/\sigma^2)$, of which $0.539(\varepsilon/\sigma^2)$ is the kinetic contribution. In the tabulated numerical results we have chosen units with $m=1$, $\varepsilon=1$, and $\sigma=1$. The total time of the run is expressed in units of $\tau=1/\dot\varepsilon$. The four simulations indicated by an asterisk (*) are in the instability region discussed in the text.

| N	t/τ	$\dot\varepsilon$	$\langle\Phi/N\varepsilon\rangle$	$\langle P_{xy}\rangle$		$\langle P_{xx}\rangle$		$\langle P_{yy}\rangle$	
1024	22	0.001	0.461	−0.0129	+0.0002	+0.5398	+0.4847	+0.5384	+0.4847
1024	16	0.002	0.461	−0.0271	+0.0003	+0.5417	+0.4847	+0.5365	+0.4848
1024	20	0.005	0.461	−0.0682	+0.0009	+0.5538	+0.4845	+0.5349	+0.4849
1024*	86	0.008	0.436	−0.1317	+0.0005	+0.901	+0.488	+0.227	+0.488
1024*	105	0.009	0.441	−0.0806	+0.0009	+0.907	+0.484	+0.212	+0.484
1024*	189	0.010	0.424	−0.1384	+0.0000	+1.055	+0.492	+0.097	+0.492
1024*	169	0.011	0.456	−0.1150	+0.0016	+0.673	+0.484	+0.415	+0.484
1024	296	0.020	0.458	−0.1802	+0.0026	+0.6774	+0.4832	+0.4078	+0.4852
1024	78	0.050	0.458	−0.2557	+0.0040	+0.7465	+0.4818	+0.3370	+0.4876
1024	308	0.100	0.458	−0.2675	+0.0042	+0.8281	+0.4802	+0.2552	+0.4900
1024	472	0.200	0.458	−0.2549	+0.0036	+0.9028	+0.4788	+0.1809	+0.4923
1024	550	0.500	0.459	−0.2124	+0.0012	+0.9761	+0.4775	+0.1057	+0.4951
4096	165	0.500	0.459	−0.2120	+0.0014	+0.9769	+0.4771	+0.1057	+0.4949
1024	760	1.000	0.462	−0.1733	+0.0016	+1.0090	+0.4764	+0.0664	+0.4971
4096	250	1.000	0.462	−0.1735	+0.0013	+1.0091	+0.4765	+0.0663	+0.4972
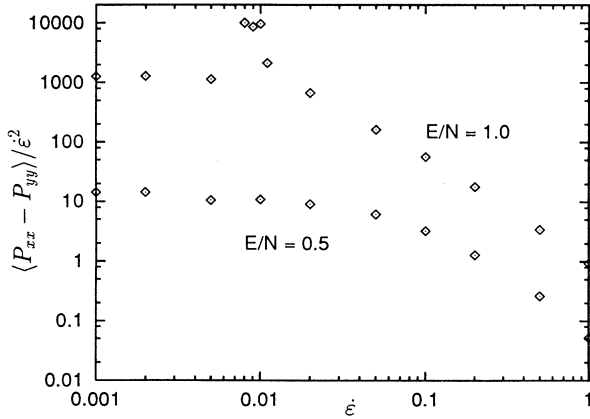
FIG. 8. Dependence of the normal stress function, $\langle P_{xx}-P_{yy}\rangle/\dot{\varepsilon}^2$, on reduced strain rate for $E=N\varepsilon$ and $E=N\varepsilon/2$, based on simulations with 1024 Lucy particles. Unit stress corresponds to ε/σ^2 while unit strain rate is $(\varepsilon/m\sigma^2)^{1/2}$.

FIG. 9. Green-Kubo integrand for 1024 Lucy particles at an energy of $E=N\varepsilon$ and unit density, $N\sigma^2=V$. The mean temperature is $0.539\varepsilon/k$ and the integrated viscosity, $14.0(m\varepsilon)^{1/2}/\sigma$, is not inconsistent with our more-extensive nonequilibrium simulations. The simulation time is $40\,000(m\sigma^2/\varepsilon)^{1/2}$. This extensive simulation was required to eliminate apparent oscillations in the correlation function. A semilogarithmic plot of the same data reveals a good straightline exponential decay up to a time of $80(m\sigma^2/\varepsilon)^{1/2}$. Here unit stress is ε/σ^2.

We expect that a similar argument would provide an effective heat conductivity for the Lucy potential, but we have not checked this notion.

V. GREEN-KUBO CORRELATION FUNCTIONS FOR LUCY'S WEIGHT FUNCTION

We found that the Green-Kubo integrand for shear viscosity, shown in Fig. 9, requires extremely long simulation times for convergence. The convergence is evidently not even relevant [4,5] for times greater than $dt/d\varepsilon$, although the plotted data suggest that exponential decay is an accurate representation for times from about $5(m\sigma^2/\varepsilon)^{1/2}$ to $80(m\sigma^2/\varepsilon)^{1/2}$. The canonical-ensemble Green-Kubo expression for shear viscosity [3,5,19] is

$$\eta=(V/kT)\int_0^\infty \langle P_{sh}(0)P_{sh}(t)\rangle_{equilibrium}dt \; , \qquad (5.1)$$

where the time-dependent pressure components P_{sh} can represent either P_{xy} or $(P_{xx}-P_{yy})/2$ in two dimensions. By comparing the two correlation functions for P_{xy} and $(P_{xx}-P_{yy})/2$, an idea of the uncertainties results. This comparison, and the long simulation times required to obtain the correlation function, suggests that nonequilibrium methods are much more efficient than the Green-Kubo approach for this soft Lucy potential.

Many theoretical investigations, summarized in Ref. [4], have concluded that two-dimensional transport coefficients are ill defined, based on the large-system divergence of the corresponding Green-Kubo expressions. On the other hand, our own investigations, past [5,15] and present, show that the two-dimensional viscosity is apparently well defined in a homogeneously ergostatted large-system "hydrodynamic limit."

The situation is still somewhat unclear, at least to us. Our own viscosity work, along with that of others [20], as well as diffusion studies, in systems with rigid boundaries, of Bocquet [21], all suggest no divergence of transport coefficients for large two-dimensional systems. Bocquet and Barrat have recently 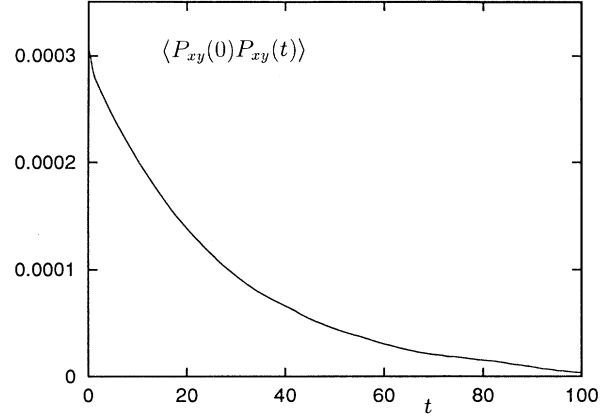published their theoretical and computational studies of boundary effects on transport in three dimensions [22]. Their two-dimensional work is in preparation.

We imagine that the theoretical predictions of divergence reflect the relative importance of fluctuations in two dimensions. In two dimensions, both boundaries and fluctuations produce effects of order $N^{1/2}$. This fact led us to study the boundary dependence of mean-squared-displacement divergence in two-dimensional crystals [15,23]. We found that this quantity diverges logarithmically for both types of boundaries, periodic and rigid, although with slightly different coefficients. It appears to us that viscosity is a useful concept in two dimensions, as it is in three. Viscosity only becomes well defined in a large-system limit which incorporates thermostats, or ergostats, to ensure a homogeneous steady state.

VI. RAYLEIGH-BÉNARD PROBLEM FOR TWO-DIMENSIONAL IDEAL GASES

What is Rayleigh-Bénard instability? If a fluid expands when heated, then the effect of gravitational forces on the resulting density gradient can lead to convection currents [24]. These convection currents, when excited, typically transport heat somewhat more efficiently than does quiescent conduction. The dependence of the problem on temperature leads to two noticeable transitions. For a nearly incompressible fluid, these transitions can be described in terms of the dimensionless Rayleigh number

$$R=g(\partial\ln V/\partial T)_p(\Delta T/L)L^4/(Dv) \; , \qquad (6.1)$$

where L is the cell height, D is the thermal diffusivity, $D=\kappa/(\rho c)$, with c the specific heat, and v is the kinematic viscosity, $v=(\eta/\rho)$. The gravitational acceleration g is

discussed below. At the critical Rayleigh number, steady convection currents form. At a considerably higher Rayleigh number, the flow becomes chaotic.

The Rayleigh-Bénard problem has been both discussed and solved, in many ways [24–27], both analytic and numerical. We imitate the conditions of a recent numerical Boltzmann-equation calculation [26] in which the material is a low-density ideal gas. We found it simpler to solve the continuum equations numerically than to attempt to extract a numerical solution from the theoretical work in Refs. [24,27]. We focus on densities and temperatures near unity. If we consider the twin effects of gravitation and a parallel temperature gradient, the vertical accelerations can be chosen to minimize density variations:

$$\rho g + (\partial P / \partial T)_\rho dT / dy = 0 \Longrightarrow g = k \Delta T / (mL) . \quad (6.2)$$

We further choose the temperature difference between the upper and lower walls equal to the mean temperature, $\Delta T = T$, so that the Rayleigh number becomes

$$R = [k \Delta T / (mLT)](\Delta T / L)L^4 / (Dv) = (L^2 kT / m) / (Dv) . \quad (6.3)$$

Chandrasekhar's analysis [24] (see also Ref. [27]) establishes that quiescent heat flow becomes unstable to convection if the Rayleigh number exceeds a critical value R_c. With the horizontal boundaries at the top and bottom of the convection cell free of friction, R_c is 658. With these boundaries rigid, with vanishing normal and tangential velocity components, the critical value is $R_c = 1708$. We choose periodic vertical boundaries (rather than the reflecting boundaries of Ref. 26), as shown in Fig. 10. This choice is the simplest consistent with Chandrasekhar's analysis. Because his choice of rigid horizontal boundaries (with v vanishing there) corresponds to an aspect ratio within a percent of 2, we adopted that choice for a numerical test of the smoothed-particle method.

The lateral periodic boundaries are straightforward to implement, and require no discussion. For reproducibility, the top-and-bottom boundary conditions need to be discussed in some detail. We consider the three steps involved in solving the smoothed-particle equations of motion: (i) calculation of densities $\{\rho_i\}$, (ii) calculation of
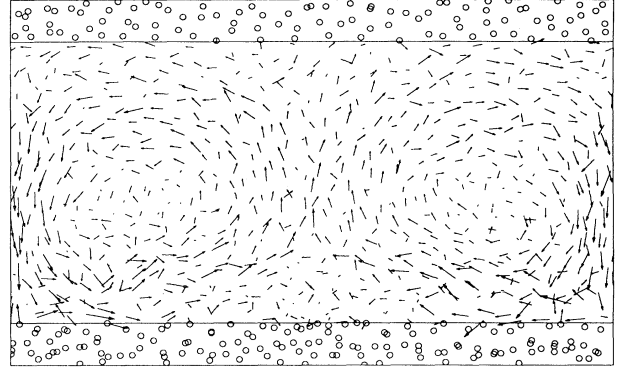

FIG. 10. Rayleigh-Bénard flow of a macroscopic ideal gas using 800 Lucy particles and smooth-particle applied mechanics: $T_{\text{hot}} = 1.5(\varepsilon / k)$, $T_{\text{cold}} = 0.5(\varepsilon / k)$, with gravitational acceleration $g = k \Delta T / mL_y$. The volume is $800\sigma^2 = L_x L_y$. The flow patterns for $(\eta / \rho) = D = \kappa / (\rho c_V) = \{0.10, 0.15, 0.20\}(\varepsilon / m)^{1/2}\sigma$ are not significantly different despite "Rayleigh numbers" of 40 000 (shown here), 22 500, and 10 000. Notice that the vertical boundaries are periodic and that reflected "image" particles enforce the horizontal top and bottom boundary conditions of fixed temperature and vanishing flow velocity. The image particles are shown as open circles.

gradients $\{(\nabla v)_i; (\nabla T)_i\}$, (iii) calculation of time derivatives $\{\dot{v}_i; \dot{e}_i\}$.

First, the densities of bulk particles inside the container include contributions from reflected image particles, as shown in Fig. 10. Next, contributions from the images are used in the calculation of the velocity and temperature gradients. In the bulk fluid, these gradients can best be calculated by starting from the identity

$$\rho \nabla f = \nabla(\rho f) - f \nabla \rho , \quad (6.4)$$

where f can represent either the velocity or the temperature. This choice leads to the highly desirable absence of flux contributions between smooth particles having the same values of f. Expressing the two gradients, on the right-hand side, in terms of the smoothed-particle weighting function w, and dividing by a symmetrized density ρ_{ij}, leads to the following definitions:

$$\left\{ (\nabla v)_i = m \sum_j [\nabla_i w_{ij}][v_j - v_i] / \rho_{ij} , \quad (\nabla T)_i = m \sum_j [\nabla_i w_{ij}][T_j - T_i] / \rho_{ij} \right\} ; \quad w_{ij} = w(r_{ij}) , \quad (6.5)$$

where ∇v is a second-rank tensor, ∇T is a vector, and where we can choose either the *arithmetic-mean* density, $\rho_{ij} = (\rho_i + \rho_j) / 2$ or the *geometric-mean* density, $\rho_{ij} = (\rho_i \rho_j)^{1/2}$. These choices lead to very similar results. For the reflected boundary contributions of $\{\tilde{i}, \tilde{j}\}$, the images of $\{i, j\}$, we include all pairs of contributions $\{\tilde{i}, j\}$ and $\{\tilde{j}, i\}$ for which a particle-image pair has a separation less than the range of the weighting function. See again Fig. 10, in which image particles are indicated by open circles. For the image of particle i, $v_{\tilde{i}}$, and $T_{\tilde{i}}$ are taken equal to the *boundary* values rather than to the bulk values v_i and T_i.

The equations of motion are based on a different identity,

$$(\nabla f) / \rho = \nabla(f / \rho) + (f / \rho^2)(\nabla \rho) , \quad (6.6)$$

where f can represent either the velocity v or the internal energy e. This choice is motivated by the fact that it leads to the conservation of f in the interaction of particle pairs. For smoothed particles in the bulk fluid, the corresponding equations of motion are

$$\left\{ d\mathbf{v}_i/dt = \sum [(m\sigma/\rho^2)_j + (m\sigma/\rho^2)_i] \cdot \nabla_i w_{ij} \right\} .$$ (6.7)

The conductive contribution to the energy change has a similar form:

$$\left\{ (de_i/dt)_{\text{conduction}} = -\sum [(m\mathbf{Q}/\rho^2)_j + (m\mathbf{Q}/\rho^2)_i] \cdot \nabla_i w_{ij} \right\} ,$$ (6.8)

where $\mathbf{Q}$ is the heat flux vector, $-\kappa\nabla T$. In these cases, the reflected image values of the stress tensor and the heat flux vector for $\{\tilde{i}, \tilde{j}\}$ are taken equal to the corresponding bulk values of particles $\{i, j\}$. In calculating the smoothed-particle boundary contribution to the compressive energy change, $\rho \, de/dt = \sigma:\nabla\mathbf{v}$, the image stresses are equal to the bulk stresses while the image velocities are given by the boundary values.

In relatively small-scale simulations of Rayleigh-Bénard flow, with 800 smoothed particles, we found that the flow field, shown in Fig. 10, was essentially independent of the "transport coefficients." We used state-independent Newtonian shear viscosity and Fourier heat conductivity throughout our work. With the three choices $\eta/\rho = D = \kappa/(\rho c) = \{0.10, 0.15, 0.20\}(\varepsilon/m)^{1/2}\sigma$, the flow fields are statistically indistinguishable from one another, and correspond to a kinetic temperature of $\sim 0.004\varepsilon/k$. This indicates that the *intrinsic* viscosity of the Lucy flow, though evidently less than our estimate for

an energy $E = N\varepsilon/2$, is still sufficiently great to exceed the *specified* viscosity, and dominates the flow. To emphasize this point, we carried out a simulation with the viscosity set equal to zero. (Thermal conductivity is still required, in order to drive the flow.) Again rolls formed, though irregularly and many in number, suggesting the presence of viscous dissipation in the smooth-particle model of an *inviscid fluid*.

A slightly larger system, with 5000 particles, is already sufficiently large to give a good representation of the macroscopic flow, accurate to a few percent. Figure 11 shows two flows, at Rayleigh numbers of 40 000 and 10 000. In order to compare these flows to the predictions of continuum mechanics, we have solved the complete compressible continuum equations on a variety of rectangular grids, using centered space differences and the fourth-order Runge-Kutta method to integrate $\partial\rho/\partial t$, $\partial\mathbf{v}/\partial t$, and $\partial e/\partial t$ to a fully converged steady state.

After several failed efforts, we found that a square grid, with $\mathbf{v}$, and e evaluated at the grid points and ρ, $\nabla\mathbf{v}$, ∇e, σ, and $\mathbf{Q}$ evaluated at the squares' centers provided a robust and stable scheme. A fully converged centered-

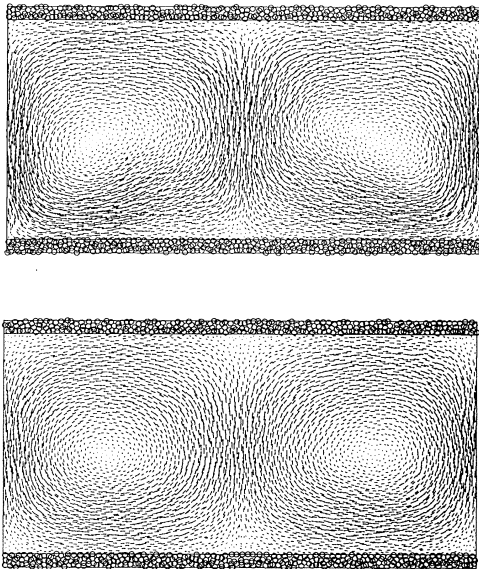FIG. 11. Rayleigh-Bénard flows of a macroscopic ideal gas using 5000 Lucy particles and smooth-particle applied mechanics: $T_{\text{hot}} = 1.5(\varepsilon/k)$, $T_{\text{cold}} = 0.5(\varepsilon/k)$, with gravitational acceleration $g = k\Delta T/mL_y$. The spatially averaged flow patterns $\{\langle \mathbf{v} \rangle\}$ for $(\eta/\rho) = D = \kappa/(\rho c_V) = \{0.25, 0.50\}(\varepsilon/m)^{1/2}\sigma$ correspond to Rayleigh numbers of 40 000 (top) and 10 000 (bottom). The volume is $5000\sigma^2 = L_x L_y$. The kinetic energy per unit mass, for the lower flow, is $0.0046(\varepsilon/m)$.
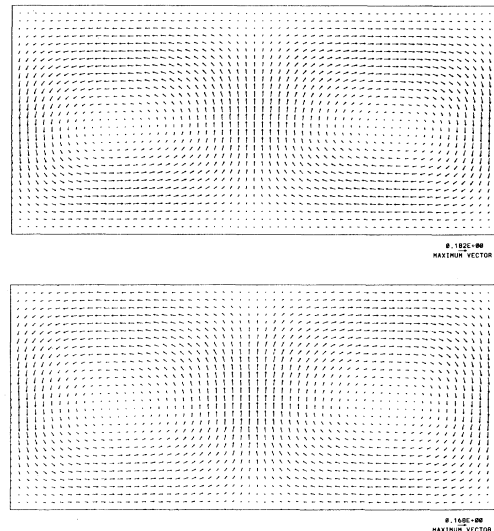

FIG. 12. Rayleigh-Bénard flow, under conditions identical to those at the bottom of Fig. 11 with a Rayleigh number of 10 000. The solution, shown at the top, was obtained by solving the compressible fluid equations on a 61×31 Eulerian mesh, using centered spatial differences and Runge-Kutta time integration. The kinetic energy per unit mass is $0.0048(\varepsilon/m)$. The solution for 5000 smoothed particles, evaluated at 1800 grid points, is shown below for comparison

difference flow field for a Rayleigh number of 10 000, corresponding to the lower illustration in Fig. 11, appears as Fig. 12. The agreement found is quite satisfactory. See the figure captions. Though smooth particles can easily produce Rayleigh-Bénard flows with a convincing appearance, using fewer particles than required by molecular dynamics simulations, quantitative results, in two dimensions, require on the order of thousands of smooth particles for velocity errors of order a few percent.

VII. CONCLUSIONS

Shear flows for the long-ranged and relatively soft Lucy potential are well described by the model of a Newtonian viscous fluid in two space dimensions. There is an interesting instability transition at relatively high energy, which deserves further study and analysis. Finite flow velocities guarantee a finite transport coefficient, even in two dimensions. The viscosities we find are essentially independent of system size and strain rate within the precision of the computer simulations. There is soon-to-be published support for this view in Green-Kubo simulations carried out by others [20]. Bocquet and Barrat, who have studied the effect of boundary conditions on transport in three dimensions [22], are now studying boundary effects in two dimensions [21]. Smooth-particle applied mechanics, which closely resembles molecular dynamics, can be used to solve continuum flow problems with fewer particles than are required for the atomistic simulations, though quantitative agreement still requires thousands of particles. See Ref. [9] for additional examples. The unusual size dependence of continuum Rayleigh-Bénard simulations, carried out with smooth-particle applied mechanics, can be understood in terms of the intrinsic viscosity due to the smooth-particle weighting function, characterized here.

[1] B. L. Holian, W. G. Hoover, and H. A. Posch, Phys. Rev. Lett. **59**, 10 (1987).

[2] W. G. Hoover, *Computational Statistical Mechanics* (Elsevier, Amsterdam, 1991).

[3] R. Zwanzig, Ann. Rev. Phys. Chem. **16**, 67 (1965).

[4] M. H. Ernst, B. Cichocki, J. R. Dorfman, J. Sharma, and H. van Beijeren, J. Stat. Phys. **18**, 237 (1978).

[5] W. G. Hoover and H. A. Posch, Phys. Rev. E **51**, 273 (1995).

[6] D. M. Gass, J. Chem. Phys. **54**, 1898 (1971).

[7] J. J. Monaghan, Ann. Rev. Astron. Astrophys. **30**, 543 (1992).

[8] O. Kum and W. G. Hoover, J. Stat. Phys. **76**, 1075 (1994).

[9] W. G. Hoover, T. G. Pierce, C. G. Hoover, J. O. Shugart, C. M. Stein, and A. L. Edwards, Comput. Math. Appl. **28**, 155 (1994).

[10] *Advances in the Free-Lagrange Method*, edited by H. E. Trease, M. J. Fritts, and W. P. Crowley, Lecture Notes in Physics Vol. 395 (Springer-Verlag, Berlin, 1991).

[11] L. B. Lucy, Astron. J. **82**, 1013 (1977).

[12] E. S. Oran and J. P. Boris, Comput. Phys. **7**, 523 (1993).

[13] U. Frisch and S. A. Orszag, Phys. Today **43**(1), 24 (1990).

[14] Y. L. Klimontovich, *Statistical Physics* (Harwood, London, 1986), Chap. 23.

[15] W. G. Hoover, W. T. Ashurst, and R. J. Olness, J. Chem. Phys. **60**, 4043 (1974).

[16] W. G. Hoover, A. J. C. Ladd, and B. Moran, Phys. Rev. Lett. **48**, 1818 (1982).

[17] S. Nosé, J. Chem. Phys. **81**, 511 (1984).

[18] W. G. Hoover, Phys. Rev. A **31**, 1695 (1985).

[19] D. J. Evans and G. P. Morriss, *Nonequilibrium Liquids* (Academic, New York, 1990).

[20] D. Gravina, G. Ciccotti, and B. L. Holian, Phys. Rev. E (to be published).

[21] L. Bocquet (private communication).

[22] L. Bocquet and J.-L. Barrat, Phys. Rev. E **49**, 3079 (1994).

[23] W. G. Hoover and O. Kum, J. Chem. Phys. (to be published).

[24] S. Chandrasekhar, *Hydrodynamic and Hydromagnetic Stability* (Clarendon, Oxford, 1961), p. 43.

[25] I. Goldhirsch, R. B. Pelz, and S. A. Orszag, J. Fluid Mech. **199**, 1 (1989).

[26] T. Watanabe, H. Kaburaki, and M. Yokokawa, Phys. Rev. E **49**, 4060 (1994).

[27] A. Schlüter, D. Lortz, and F. Busse, J. Fluid Mech. **23**, 129 (1965).